J Solid State Electrochem (2010) 14:1615–1620
DOI 10.1007/s10008-010-1003-2

ORIGINAL PAPER

# Preparation and characterization of AuPt alloy nanoparticle–multi-walled carbon nanotube–ionic liquid composite film for electrocatalytic oxidation of cysteine

**Zhirong Mo · Faqiong Zhao · Fei Xiao · Baizhao Zeng**

Received: 21 August 2009 / Revised: 26 December 2009 / Accepted: 3 January 2010 / Published online: 27 January 2010


**Abstract** Gold–platinum (AuPt) alloy particles were fabricated directly on multi-walled carbon nanotubes (MWNT)–ionic liquid (i.e., trihexyltetradecylphosphonium bis(trifluoromethylsulfonyl)imide, $[P_{6,6,6,14}][NTf_2]$) composite coated glassy carbon electrode (GCE) by electrodeposition method. Scanning electron microscope image showed that they were well-dispersed nanocluster consisting of smaller nanoparticles, and their size was about 70 nm. X-ray diffraction experiment showed that they were single-phase alloy nanomaterial, and the calculated composition was consisting with that obtained by energy dispersive X-ray spectroscopy. The resulting modified electrode (i.e., AuPt–MWNT–$[P_{6,6,6,14}][NTf_2]$/GCE) presented high catalytic activity for the electrochemical oxidation of cysteine. The peak potential of cysteine shifted to 0.42 V (versus saturated calomel electrode) in 0.1 M $H_2SO_4$ and the peak current increased greatly in comparison with that on the corresponding Pt (or Au)–MWNT–$[P_{6,6,6,14}][NTf_2]$/GCE. Under the optimized conditions, the oxidation current of cysteine at 0.45 V was linear to its concentration in the range of $5.0\times10^{-7}$~$4.0\times10^{-5}$ M with a sensitivity of 43.8 mA $M^{-1}$.

**Keywords** Gold–platinum alloy nanoparticle · Ionic liquid · Carbon nanotube · Cysteine · Electrocatalysis

Z. Mo · F. Zhao · F. Xiao · B. Zeng (✉)
College of Chemistry and Molecular Sciences, Wuhan University, Wuhan, Hubei Province 430072, People's Republic of China
e-mail: bzzeng@whu.edu.cn

## Introduction

Cysteine is an important amino acid and its study and detection have received much attention [1]. Voltammetry is a sensitive and convenient method for the determination of many species. Unfortunately, cysteine cannot cause good response at ordinary electrodes such as Pt, Au, carbon paste, and graphite electrode [2]. To improve the situation, several chemically modified electrodes were developed for the electrochemical oxidation and detection of cysteine [3–5]. However, the modified electrodes still have disadvantages such as leaching of electron transfer mediator and poor long-term stability. Furthermore, the preparation methods are complicated [6]. Hence, it is pertinent to explore new methods to fabricate modified electrodes with high efficiency for the electrocatalytic oxidation of cysteine.

Pt-based alloy nanomaterials show excellent catalytic activity and stability, and they are widely studied in recent years [7]. Among them, PtAu bimetallic nanoparticle (NP) has been used as catalyst for alkane conversion [8], NO reduction [9], $CH_3OH$ oxidation [10], and glucose oxidation [11]. Pt-based alloy nanomaterials can be fabricated through different methods, such as chemical coreduction [12], hydrogen reduction [13], and two-step pyrolysis process [14]. Electrodeposition method is also among them. In our previous work, well-dispersed Pt-based alloy nanoparticles were fabricated through electrodeposition, and the resulting alloy nanoparticle-coated electrodes exhibited excellent catalysis to the electrochemical oxidation of nitrite and $H_2O_2$ [15, 16]. As the properties of metallic nanoparticles depend on their size and shape [17, 18], the fabrication method does influence their catalytic activity and thus receive much attention.

Carbon nanotubes (CNTs) have high electrical conductivity, high catalytic activity, and large specific surface area, so they are widely used to fabricate modified electrode and supporting material. Ionic liquids (ILs) are liquid substance composed entirely of ions. They can be used to immobilize other materials by binding and to fabricate nanomaterial. ILs still can promote electron transfer and accumulate analytes [19]. Considering the characteristics of CNTs and ILs, some researchers tried to construct electrochemical sensors using CNT–IL composite and interesting results were obtained. In addition, CNT–IL composite was considered as good supporting material for electrodeposition of metallic nanoparticles [15, 16].

In this work, the electrochemical oxidation of cysteine on AuPt alloy nanoparticles electrodeposited on CNT–IL composite substrate is explored for the first time. Experiment shows that the as-made AuPt–MWNT–[$P_{6,6,6,14}$][$NTf_2$]/GCE possesses high stability and remarkable catalytic activity for the electrochemical oxidation of cysteine.

## Experimental

### Reagents and apparatus

The multi-walled carbon nanotube used (diameter: 10~30 nm, length: 0.5~40 nm, purity: ≥95%) came from Shenzhen Nanotech Port Co., Ltd. (Shenzhen, People's Republic of China). [$P_{6,6,6,14}$][$NTf_2$] was purchased from Sigma–Aldrich, and it was used as received. Cysteine, $H_2PtCl_6 \cdot 6H_2O$, $HAuCl_4 \cdot 4H_2O$, and *N*,*N*-dimethylformamide (DMF) were obtained from Sinopharm Chemical Reagent Co., Ltd. (Shanghai, People's Republic of China). Other reagents used were of analytical grade, and the water was redistilled.

Electrodeposition, cyclic voltammetric (CV), and chronoamperometric experiments were performed with a CHI 830 electrochemical workstation (CH Instrument Company, Shanghai, People's Republic of China). A conventional three-electrode system was adopted. The working electrode was a modified GCE (3 mm in diameter) or a modified glass substrate (10 mm×30 mm×2.2 mm) coated with a fluorine-doped tin oxide film (FTO: 150 nm, 20 Ω), the auxiliary and reference electrodes were a platinum wire and a SCE, respectively. The scanning electron microscope (SEM) image was obtained using a HITACHI X–650 SEM (Hitachi Co., Japan), with energy dispersive X-ray spectroscopy meter for elemental chemical analysis. The X-ray diffraction (XRD) data were collected with a Rigaku D/max-rA diffractometer (Japan) using Cu KR radiation (40 kV, 200 mA) with a Ni filter. All measurements were conducted at room temperature.

### Preparation of modified electrode

Firstly, 1.0 mg MWNT was dispersed in 1.0 ml DMF with the aid of ultrasonic agitation. Then 10.0 μl [$P_{6,6,6,14}$][$NTf_2$] was introduced to the mixture under stirring. Three microliters of the suspension was dropped on a cleaned GCE or a FTO and then dried under an infrared lamp. Thus a uniform film-coated electrode (i.e., MWNT–[$P_{6,6,6,14}$][$NTf_2$]/GCE (or FTO)) was obtained. MWNT/GCE (or FTO) and [$P_{6,6,6,14}$][$NTf_2$]/GCE (or FTO) were prepared through a similar procedure. The electrodeposition of AuPt alloy nanoparticles on MWNT–[$P_{6,6,6,14}$][$NTf_2$]/GCE (or FTO) was performed in a 0.2 M $H_2SO_4$ aqueous solution containing 1.0 mM $HAuCl_4$ and 1.0 mM $H_2PtCl_6$, the potential was −0.25 V and the time was 500 s [20, 21]. The obtained AuPt–MWNT–[$P_{6,6,6,14}$][$NTf_2$]/GCE (FTO) was washed carefully with redistilled water and then dried at room temperature. The AuPt/GCE (FTO), AuPt–MWNT/GCE (FTO), AuPt–[$P_{6,6,6,14}$][$NTf_2$]/GCE (FTO), Au–MWNT–[$P_{6,6,6,14}$][$NTf_2$]/GCE (FTO), and Pt–MWNT–[$P_{6,6,6,14}$][$NTf_2$]/GCE (FTO) were fabricated through a similar method. Prior to the experiments, the solution was deoxygenated with nitrogen gas.

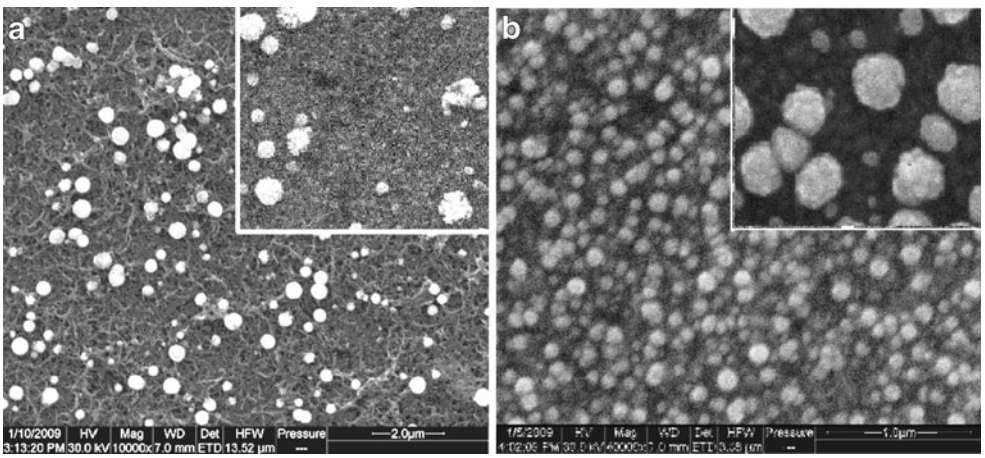


**Fig. 1** SEM images of AuPt alloy particles deposited on bare FTO (**a**, *inset*), MWNT/FTO (**a**), [$P_{6,6,6,14}$][$NTf_2$]/FTO (**b**, *inset*) and MWNT–[$P_{6,6,6,14}$][$NTf_2$]/FTO (**b**). Solution composition: 0.2 M $H_2SO_4$ aqueous solution containing 1.0 mM $HAuCl_4$ and 1.0 mM $H_2PtCl_6$; deposition potential: −0.25 V

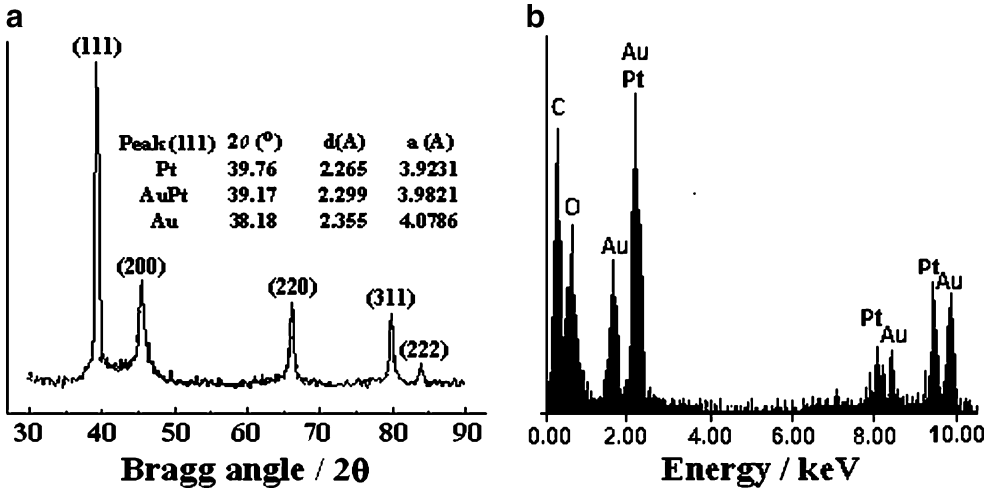


**Fig. 2** XRD patterns of AuPt particles deposited on MWNT–$[P_{6,6,6,14}][NTf_2]$ film (**a**); EDS of AuPt particles deposited on MWNT–$[P_{6,6,6,14}][NTf_2]$ film (**b**)

## Results and discussion

### Morphological analysis

The images of AuPt alloy deposited on bare FTO, MWNT/FTO, $[P_{6,6,6,14}][NTf_2]$/FTO, and MWNT–$[P_{6,6,6,14}][NTf_2]$/FTO are presented in Fig. 1. Compared with the AuPt alloy deposited on bare FTO (Fig. 1a, inset), the particle density of AuPt alloy on MWNT/FTO increases and the particle size decreases (Fig. 1a), demonstrating that MWNT is favorable for the nucleation of metal. The sizes of AuPt alloy particles deposited on the $[P_{6,6,6,14}][NTf_2]$/FTO (average diameter of 250 nm) and MWNT–$[P_{6,6,6,14}][NTf_2]$/FTO (average diameter of 70 nm) are still smaller. Especially, the AuPt particles deposited on MWNT–$[P_{6,6,6,14}][NTf_2]$/FTO are uniform and close-packed. This means that $[P_{6,6,6,14}][NTf_2]$ can make the particle size decrease and promote the particle dispersion. This phenomenon can be explained as follows: $[P_{6,6,6,14}][NTf_2]$ has high viscosity and can prevent the particles from aggregating; on the other hand, $[P_{6,6,6,14}][NTf_2]$ may interact with Au and Pt, forming a protecting layer outside the AuPt particles and making them stable.

### Structure and composition analysis

To estimate the structure and composition of AuPt alloy particles, they are characterized by XRD (Fig. 2a). As can be seen, the pattern of AuPt particles exhibits five major peaks, which can be assigned to AuPt (111), −(200), −(220), −(311), and −(222) planes of the face-centered cubic lattice of AuPt alloy. These peaks perfectly fit a single analytical function, suggesting that they are single-phase nanomaterial, i.e., AuPt alloy [22]. Compared with that of pure Pt (JCPDS 04–0802), the shift of the (111) peak to lower $2\theta$ angle could be indexed to a higher $d$ space ($d_{111}$=2.299 Å) crystal structure. The lattice constant for the fcc-type AuPt phase is $a$=3.9821 Å, which is measurably larger than that of pure Pt ($a$=3.9231 Å) but smaller than that of pure Au (JCPDS 04–0784, $a$=4.0786 Å). This result confirms the formation of AuPt alloy [22].

Based on Scherrer formula [23], $L=0.9\ \lambda K_{a1}/B_{(2\theta)}\cos\theta_B$, where $L$ is the average size of particles, $\lambda k_{a1}$ is the X-ray wavelength, $B_{(2\theta)}$ is the peak broadening, and $\theta_B$ is the angle of the peak maximum. Here, the mean diameter of the AuPt alloy NPs estimated from the half-width of the (111)

**Table 1** Surface area of alloy NPs calculated according to CV and XRD analysis and composition of different alloy NPs estimated from XRD, EDS, and CV analysis

| Electrode | $S_{EAS}$ ($m^2g^{-1}$) | $S_{CSA}$ ($m^2g^{-1}$) | $\Theta$ | Composition | | |
|---|---|---|---|---|---|---|
| | | | | XRD | EDS | CV |
| AuPt/GCE | 16.1 | – | – | $Au_{41}Pt_{59}$ | $Au_{44}Pt_{56}$ | $Au_{22}Pt_{78}$ |
| Pt–MWNT–$[P_{6,6,6,14}][NTf_2]$/GCE | 12.5 | 4.03 | 3.10 | – | – | – |
| AuPt–MWNT–$[P_{6,6,6,14}][NTf_2]$/GCE | 25.6 | 4.62 | 5.54 | $Au_{38}Pt_{62}$ | $Au_{43}Pt_{57}$ | $Au_{15}Pt_{85}$ |

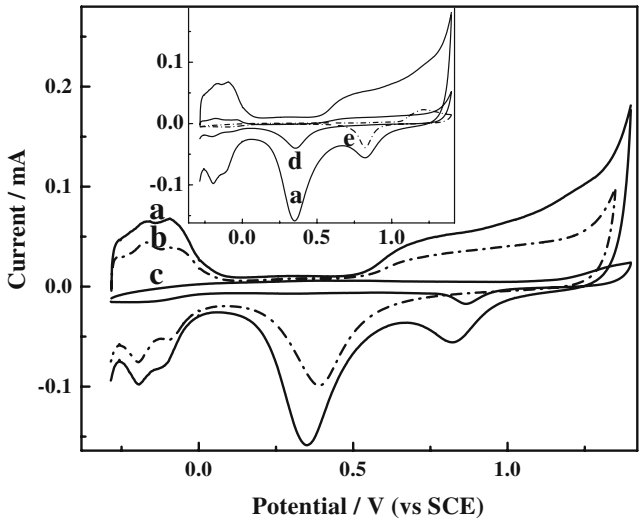


**Fig. 3** Cyclic voltammograms of AuPt–MWNT–[$P_{6,6,6,14}$][$NTf_2$]/GCE (*a*), Pt–MWNT–[$P_{6,6,6,14}$] [$NTf_2$]/GCE (*b*), Au–MWNT–[$P_{6,6,6,14}$][$NTf_2$]/GCE (*c*), Pt/GCE (*d*), and Au/GCE (*e*) in deaerated 0.1 M $H_2SO_4$ solutions. Scan rate is 100 mV $s^{-1}$

diffraction peak is 63 nm, which is in good agreement with the SEM result.

The total surface area of corresponding alloy NPs can also be estimated from the XRD peaks through the following equation [7, 24]: $S_{CSA}=6000/\rho d$, where $d$ is the average particle size (nm) and $\rho$ is the density ($\rho_{Pt}$=21.4 g $cm^{-3}$, $\rho_{Au}$=19.32 g $cm^{-3}$, and $\rho_{alloy} = W_{Pt}\% \times \rho_{Pt} + W_{Au}\% \times \rho_{Au}$, where $W$% means weight percent). The calculated values of $S_{CSA}$ are summarized in Table 1.

Assuming the validity of Vegard's law (the linear lattice constant–concentration relation) [23], one can estimate the composition of the alloy. The results are shown in Table 1. The composition of the resulting alloy is also analyzed by EDS as shown in Fig. 2b. The result is consisting with that obtained by XRD.

## Electrochemical characterization of AuPt–MWNT–[$P_{6,6,6,14}$][$NTf_2$]/GCE

Figure 3 shows the voltammograms of AuPt–MWNT–[$P_{6,6,6,14}$][$NTf_2$]/GCE, Pt–MWNT–[$P_{6,6,6,14}$][$NTf_2$]/GCE, Au–MWNT–[$P_{6,6,6,14}$][$NTf_2$]/GCE, Pt/GCE, and Au/GCE in a deaerated 0.1 M $H_2SO_4$ solution. The peaks characterizing the hydrogen adsorption/desorption and oxide formation/stripping of Pt and Au can be observed. The integrated charge of the hydrogen absorption peak permits an estimate of the electrochemically active surface area ($S_{EAS}$) [7], $S_{EAS} = Q_{ads}/Q_{ref}L_{Pt}$, where $Q_{ads}$ is the integrated charge of hydrogen absorption peak, $Q_{ref}$ is the hydrogen adsorption charge on a smooth platinum electrode (0.21 mC $cm^{-2}$) and $L_{Pt}$ is the Pt loading. $S_{EAS}$ values are displayed in Table. 1. The $S_{EAS}$ of AuPt–MWNT–[$P_{6,6,6,14}$][$NTf_2$]/GCE is much larger than that of AuPt/GCE due to more AuPt depositing on the MWNT–[$P_{6,6,6,14}$][$NTf_2$]/GCE. On the other hand, the $S_{EAS}$ of AuPt–MWNT–[$P_{6,6,6,14}$][$NTf_2$]/GCE is about 2.0 times of that of Pt–MWNT–[$P_{6,6,6,14}$][$NTf_2$]/GCE, indicating that Au can improve the electrochemical activity.

The charge associated with the reduction of oxide species of the electrode surface can be used to determine the surface composition. The peak around 0.35 V versus SCE during negative sweep is associated with Au species, whereas the one at 0.83 V versus SCE corresponds to Pt

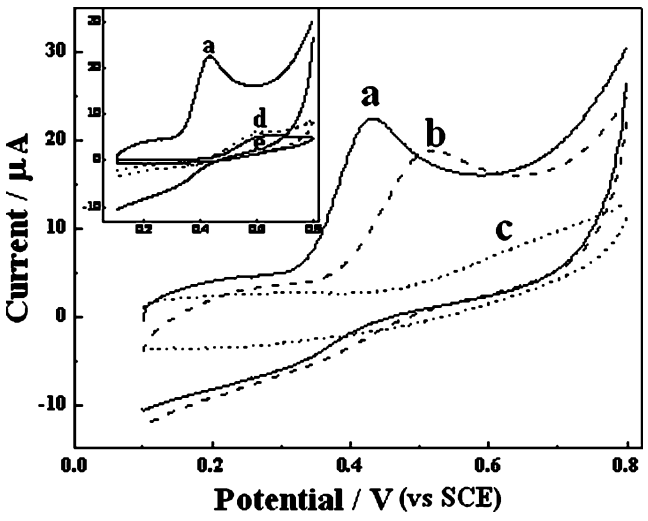


**Fig. 4** Cyclic voltammograms of cysteine at AuPt–MWNT–[$P_{6,6,6,14}$][$NTf_2$]/GCE (*a*), Pt–MWNT–[$P_{6,6,6,14}$][$NTf_2$]/GCE (*b*), Au–MWNT–[$P_{6,6,6,14}$][$NTf_2$]/GCE (*c*), Pt (*d*), and Au (*e*) electrodes. Solution composition is $5.0\times10^{-4}$ M cysteine plus 0.1 M $H_2SO_4$; scan rate is 100 mV $s^{-1}$

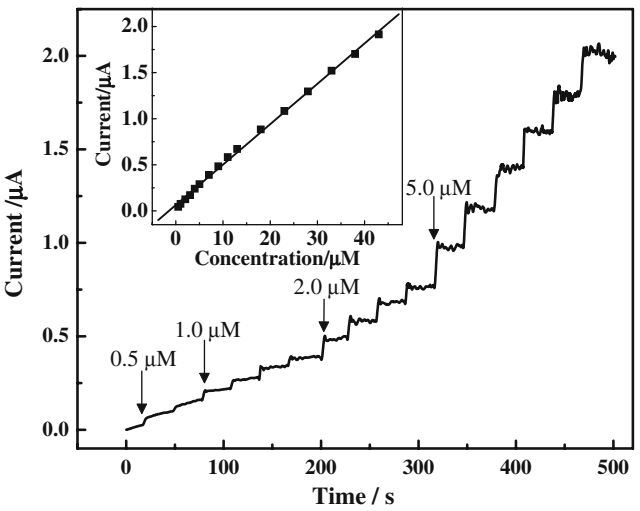


**Fig. 5** Amperometric response of AuPt–MWNT–[$P_{6,6,6,14}$][$NTf_2$]/GCE to successive addition of 0.5, 1.0, 2.0, and 5.0 μM cysteine. Applied potential: 0.45 V; supporting electrolyte: 0.1 M $H_2SO_4$. *Inset*: plot of current versus cysteine concentration

species. For pure catalysts, the charge values of 493 and 543 μC $cm^{-2}$ are obtained for Pt and Au, respectively. The atomic content of the AuPt NPs can be deduced as follows [11]: $x = S_{Au}/S_{Au} + S_{Pt}$, where $x$ represents the Au content, and $S_{Au}$ and $S_{Pt}$ are the electrode surface covered by gold and platinum oxides, respectively. The results obtained are summarized in Table 1. It can be noted that there is an inconsistency between the composition data estimated from XRD, energy dispersive X-ray spectroscopy, and CV. This is because XRD compositional analysis refers to the crystalline part of the sample, while EDS characterizes the entire sample and the CV data are related to the surface composition.

### Electrocatalytic oxidation of cysteine at AuPt–MWNT–$[P_{6,6,6,14}][NTf_2]$/GCE

The cyclic voltammograms of cysteine at AuPt–MWNT–$[P_{6,6,6,14}][NTf_2]$/GCE, Pt–MWNT–$[P_{6,6,6,14}][NTf_2]$/GCE, and Au–MWNT–$[P_{6,6,6,14}][NTf_2]$/GCE are displayed in Fig. 4. It can be seen that cysteine exhibits an irreversible anodic peak at these electrodes, but the peak potential and peak current are different. At the conventional Au and Pt electrodes, the oxidation peak is very small and broad, the peak potential is above 0.6 V. Similar phenomenon is observed for the Au–MWNT–$[P_{6,6,6,14}][NTf_2]$/GCE. This means that these electrodes have poor catalysis to the electrochemical oxidation of cysteine. However, at the Pt–MWNT–$[P_{6,6,6,14}][NTf_2]$/GCE the anodic peak increases greatly and the peak potential shifts negatively to 0.50 V, reflecting the good catalysis of Pt nanoparticles. Cysteine exhibits still bigger peak at the AuPt–MWNT–$[P_{6,6,6,14}][NTf_2]$/GCE, and the peak potential lowers to 0.42 V further. It indicates that the AuPt alloy has higher electrocatalytic activity towards cysteine oxidation. As the eletrocatalytic activity of AuPt alloy nanoparticles is better than that of monometallic counterpart, the synergistic effect of Au and Pt in the alloy nanoparticles is proposed to account for this phenomenon.

### Influence of solution pH and scan rate

The influence of pH on cysteine oxidation was also studied. The anodic peak potential shifted negatively and the peak current decreased dramatically with increasing pH. Furthermore, when pH exceeded 7.0, no discernable peak occurred. Thus 0.1 M $H_2SO_4$ was used as electrolyte in this work. At the AuPt–MWNT–$[P_{6,6,6,14}][NTf_2]$/GCE, the peak potential ($E_p$) of cysteine shifted in positive direction when scan rate ($v$) increased. The $E_p$ and log$v$ showed a linear relationship, the regression equation was $E_p = 0.522 + 0.0572 \log v$ ($E_p$: V, $\nu$: V $s^{-1}$, $r$=0.998).

### Reproducibility, stability, and repeatability of AuPt –MWNT–$[P_{6,6,6,14}][NTf_2]$/GCE

The reproducibility and stability of AuPt–MWNT–$[P_{6,6,6,14}][NTf_2]$/GCE were tested. It was found that the relative standard deviation (RSD) of current was 3.2% for the amperometric response of $5\times10^{-6}$ M cysteine on five different AuPt–MWNT–$[P_{6,6,6,14}][NTf_2]$/GCE electrodes at 0.45 V. The oxidation peak current of cysteine remained more than 95% of the initial value after the modified electrode was stored for 15 days. When cyclic scan was repeated successively, the peak of cysteine slightly decreased, probably due to the accumulation of the oxidation product of cysteine on the composite electrode. However, under stirring this problem could be overcome. The RSD of response current ($n$=5) is 2.1% for successive addition of $5\times10^{-6}$ M cysteine. The AuPt–MWNT–$[P_{6,6,6,14}][NTf_2]$/GCE retains about 97% and 95% of its initial sensitivity after being used for 30 and 60 times, respectively.

### Variation of response current with cysteine concentration

Figure 5 illustrates the current variation with successive addition of cysteine to a stirred 0.1 M $H_2SO_4$. Under the optimized conditions, the response time is about 3 s, the response current is linear to cysteine concentration in the range of $5.0\times10^{-7}\sim4\times10^{-5}$ M with a regression equation of $I = 0.064 + 0.044c$ ($I$: μA, $c$: μM, $r$=0.999).

## Conclusions

AuPt alloy particles were fabricated on MWNT–$[P_{6,6,6,14}][NTf_2]$ composite film through electrodeposition method. The as-made AuPt alloy was a well-dispersed nanocluster consisting of smaller nanoparticles. Multi-walled carbon nanotube was favorable for the nucleation of AuPt; ionic liquid could promote the electrochemical deposition and dispersion of AuPt nanoparticles. The resulting AuPt–MWNT–$[P_{6,6,6,14}][NTf_2]$/GCE electrode presented high stability and catalysis for the electrochemical oxidation of cysteine.

**Acknowledgments** The authors appreciate the support of the National Natural Science Foundation of China (no. 20173040) and the State Key Laboratory of Electroanalytical Chemistry (no. 200805), Changchun Institute of Applied Chemistry, People's Republic of China.

## References

1. De Viries N, De Flora S (1993) J Cell Biochem 51:271
2. Wang ZL, Pang DW (1990) J Electroanal Chem 283:349

3. Yosypchuk B, Novotny I (2002) Talanta 56:971
4. Salimi A, Hallaj R (2005) Talanta 66:967
5. Limson J, Nyokong T (1997) Electroanalysis 9:255
6. Mazloum Ardakani M, Rahimi P, Ebrahimi Karami P, Zare HR, Naeimi H (2007) Sensors and Actuators B 123:763
7. Xu YH, Lin XQ (2007) J Power Sources 170:13
8. Song CR, Ge QF, Wang LC (2005) J Phys Chem B 109:22341
9. Mihut C, Descorme C, Duprez D, Amiridis MD (2002) J Catal 212:125
10. Luo J, Maye MM, Kariuki NN, Wang L, Njoki P, Lin Y, Schadt M, Naslund HR, Zhong CJ (2005) Catal Today 99:291
11. Habrioux A, Sibert E, Servat K, Vogel W, Kokoh KB, Alonso-Vante N (2007) J Phys Chem B 111:10329
12. Huang JE, Guo DJ, Yao YG, Li HL (2005) J Electroanal Chem 577:93
13. Watanabe M, Uchida M, Motoo S (1987) J Electroanal Chem 229:395
14. Yao YL, Ding Y, Sheng L, Xia XH (2006) Carbon 44:61
15. Xiao F, Zhao FQ, Mei DP, Mo ZR, Zeng BZ (2009) Biosens Bioelectron 24:3481
16. Xiao F, Zhao FQ, Zeng JJ, Zeng BZ (2009) Electrochem Commun 11:1550
17. Thangavel S, Ramaraj R (2008) J Phys Chem C 112:19825
18. Riu J, Maroto A, Rius FX (2006) Talanta 69:288
19. Silvester DS, Compton RG (2006) Zeitschrift Fur Ur Physikalische Chemie-International J Res Phys Chem & Chem Phys 220:1247
20. Xiao F, Zhao FQ, Zhang YF, Guo GP, Zeng BZ (2009) J Phys Chem C 113:849
21. Xiao F, Mo ZR, Zhao FQ, Zeng BZ (2008) Electrochem Commun 10:1740
22. Xu JB, Zhao TS, Liang Z, Zhu LD (2008) Chem Mater 20:1688
23. Radmilovic V, Gasteiger HA, Ross PN (1995) J Catal 154:98
24. Klug HP, Alexander LE (1974) In X-ray diffraction procedures for polycrystalline and amorphous materials, 2nd edn. Wiley, New York, 562